Electronic Supporting Information

Self-Assembly Dynamics and Accumulation Mechanisms of Ultra-Fine Nanoparticles

Noushin Nasiri, Tobias D. Elmøe, Yun Liu, Qing H. Qin, Antonio Tricoli

Correspondence to: antonio.tricoli@anu.edu.au

I. Computational Model Outline

Fig. S1 shows a schematic of a simulation domain consisting of drop and deposition cell. The particles are monodisperse with a constant diameter (5, 10, 30 and 50 nm) and a solid density of 1000 kg.m^{-3}. Particle dynamics is modeled for isothermal condition at 298 K and considering deposition of one particle at a time. In order to obtain true random motion before deposition, a particle is initially released in a cell where particle deposition and film growth are not allowed (Fig. S1, drop domain). The drop domain is always kept to $20d_p$ during all simulations. The next particle is released after deposition of the previous one. Deposition occurs when a particle touches another particle or the horizontal surface at the end of the deposition domain using a sticking coefficient of 100%. Electrical charge, Van der Walls force and extra inter-molecular forces are neglected. Surface-bond agglomerates were identified by a subroutine determining the neighboring particles having a physical connection. More details about the model outline are reported elsewhere[27].

II. Experimental: Péclet-Number Computation

Péclet-number is a non-dimensional number defined as:

$$Pe = \frac{(d_p / 2)v}{D_p} \tag{S1}$$

where d_p is the particle diameter, v is the particle translational velocity and D is the diffusion coefficient. The diffusion coefficient, D, of a particle in a fluid is calculated by the Stokes-Einstein equation:

$$D = \frac{K_b T}{f} \tag{S2}$$

where K_b is the Boltzmann constant ($1.3806488 \times 10^{-23}$ m^{2}kg.s^{-2}K^{-1}), T is the temperature and f is the friction coefficient of the particle in the fluid. In continuum (k_n << 1), transition ($k_n \approx 1$), and free molecular regime (k_n >> 1), where the friction coefficient, f, is calculated by:

$$f = 3\pi \mu d_p \qquad \text{for } k_n \ll 1 \tag{S3}$$

$$f = \frac{3\pi\mu d_p}{C_c} \qquad \text{for } k_n \approx 1 \text{ and } k_n >> 1 \tag{S4}$$

where μ is the viscosity of the medium, d_p is the particle diameter, k_n is the Knudsen number ($k_n = 2\lambda_{gas}/d_p$, λ_{gas} is the gas molecule mean free path), and C_c is the Cunningham correction factor which is equal to:

$$C_c = 1 + k_n(A_1 + A_2 e^{-\frac{2A_3}{k_n}}) \tag{S5}$$

where the values for A_1, A_2 and A_3 in the air are equal to 1.21, 0.40 and 0.78, respectively. The aerosol temperature (T_F) near the substrate is 773 K as experimentally presented. The fluid dynamic viscosity (μ_F) at 773 K and C_c for k_n of 10-100 are 3.481×10^{-5} kg.m^{-1}.s^{-1} and 100 respectively. This calculation leads to a friction and diffusion coefficient of 1.64×10^{-14} kg.s^{-1} and 6.5×10^{-7} m^2.s^{-1} which is in agreement with D reported by other researchers[20,29]. In the absence of electrical forces, the main nanoparticle deposition mechanisms are Brownian diffusion, thermophoresis and impaction. The thermophoretic velocity, v_T, is usually described as[20]:

$$v_T = -k_T \frac{\mu_F (T_F - T_S)}{\rho_F \delta_T T_P} \tag{S6}$$

where T_P is the particle temperature (approximated by the average of the aerosol (T_F) and surface (T_S) temperatures), ρ_F is the fluid density, δ_T is the boundary layer thickness and k_T is the thermophoretic coefficient which is usually assumed independent of the particle size equal to 0.55. A surface temperature (T_S) of 410 K, a small boundary layer thickness between 0.01-1 mm and the air density of 0.4565 kg.m^{-3} at 773 K. This leads to an advective velocity of 2.57 m.s^{-1}.Using diffusion coefficient of 6.5×10^{-7} m^2.s^{-1} results in a Péclet-number between 10^{-3}-10^{-1}.

III. Simulation Domain Optimization

For small Péclet-numbers, the advective velocity is nearby zero resulting in a diffusion driven deposition (diffusive regime/limit). For large Péclet-numbers, the advective velocity is dominant resulting in a ballistic limited deposition (ballistic regime). The simulations were repeated five times to obtain statistically relevant morphologies. The resulting particle distributions were investigated as a function of the total film thickness (F_d) and deposition surface size (Fig. S2a, b). The side (L_d) of the square deposition surface was increased from $20d_p$ to $140d_p$ (Fig. S2a, b) to assess the impact of geometrical simulation constrains on the resulting film morphology (Fig. S2a, b, insets). In the diffusion regime, the average film porosity (ε_{film}), calculated from 5 independent simulations, decreased rapidly with increasing total film thickness (Fig. S2a) reaching a minimum between 0.5 and 1 μm. Further increasing the film thickness resulted in a slow quasi-asymptotic porosity increase. This porosity profile was consistent for all deposition surface size (Fig. S2a, empty and full circles). However, its magnitude varied substantially with the deposition surface dimension. Increasing the surface side from $20\mathrm{d_p}$ (Fig. S2a, empty circles) to $140d_p$ (full circles) increased the minimal ($\varepsilon_{\mathrm{min}}$) and quasi-asymptotic ($\varepsilon_{\mathrm{q\text{-}a}}$) porosities from 0.966 to 0.983 and 0.973 to 0.987, respectively. This represents an up to 59% variation in film density and indicates that the deposition surface size has a considerable impact on the resulting film properties. This is in line with previous particle dynamics simulations (Table 1, main text) and partially explains the considerable higher film densities reported in the diffusion regime for small deposition surface ($L_d = 30d_p$)[21, 24, 25].

A different dependency from the simulation constrains was observed in the ballistic regime. There, the average porosity profiles (Fig. S2b) did not feature a minimum but decreased monotonously with increasing total film thickness converging to a quasi-asymptotic value of 0.865 and 0.857 for a deposition surface side of $20d_p$ and $140d_p$, respectively. This corresponded to a maximal film density variation of 5.9% and thus 10 times smaller than that in the diffusion regime. Detailed analysis of the film morphologies (Fig. S2a, b, insets) revealed that, upon deposition of the first particle layer, main agglomerates forms orthogonally from the deposition surface. These growths by collecting most of the incoming particle flux; effectively shadowing the deeper film layers. The differences observed in the diffusion and ballistic regimes are attributed to the different horizontal spread (surface density) of these surface-bonded agglomerates.

In the diffusion regime, sufficiently large deposition surfaces enabled to simulate both inter- and intra-agglomerate film porosities (Fig. S2a, inset ii). In contrast, a small deposition surface restricted the film morphology to that of single agglomerate (Fig. S2a, inset i) forcefully increasing the resulting film density. This was not the case for the ballistic regime (Fig. S2b) as the resulting agglomerate horizontal spread was considerably smaller. As a result in the ballistic limit, both small (inset i) and large (inset ii) deposition surfaces were able to capture the inter- and intra-agglomerate film porosities. This was further supported by visual rendering of the deposited particle three-dimensional distributions (Fig. S2b, insets). These showed nearly indistinguishable film morphologies for large and small deposition surfaces. For all deposition conditions ($10^{-7} \leq \mathrm{Pe} \leq 100$), it was found that the average film porosity (Fig. S3a, b) increased with increasing deposition surface dimension and converged for $L_d \geq 100d_p$. This is in line with previous particle dynamics results[23,27]showing consistent film densities for a simulation surface side larger than $100d_p$ (Table 1, main text). As a result, here, further investigation of the deposition dynamics was conducted with a large simulation surface size of $140\mathrm{d}_\mathrm{p}$ that enabled the self-assembly of more realistic film structures.

Increasing the Pe number from 10^{-7} (Fig. S3a, pure diffusion regime) to 100 (Fig. S3b, pure ballistic regime) leads to decreasing the porosity of composed film at all surface sizes. This significant change is attributed to the deposition style of the particles during transition from diffusion to the ballistic regime. In fact, at a small Pe number the particle transport is dominated by diffusion and its movement is scattered towards the deposition surface. In that case, the deposited film grows with a fractal-like structure.

IV. Validation

Fig. S4 shows the values for plateau packing density as a function of the Pe number for particle diameter of 50 nm in comparison to Rodriguez-Perez et al.[23] and Castillo et al.[28] on flat surface deposition and Elmøe et al.[27] on a porous substrate. The resulted packing density is in agreement with these results. Rodriguez-Perez et al.[23] and Castillo et al.[28] studied the particle deposition on a flat surface with structured grid domain resulting in an increase of order and density. Elmøe et al.[27] simulated the particle deposition on a porous capillary substrate. The domain length used by both researches was sufficiently large ($512d_p$ and $80d_p$)[23,27,28] leading to a good agreement with the results presented here. While, for Dreyer et al.[24] and Ogunsola et al.[22], the domain length was not sufficiently resulting lower final porosities ($30d_p$ and $40d_p$ respectively) (Table 1, main text).

V. Analytical Model

The different mechanisms for particle deposition at ballistic, randomly oriented ballistic and diffusion regimes is shown in supplementary Fig. 6. The scaled particle surface density (SD) is computed as a ratio of horizontal area shadowed by a deposited particle to that required for a particle to deposit. The horizontal area shadowed by a particle with the diameter of d_p is calculated from the following equation (Fig. S6a, insets):

$$A_{dp} = \frac{\pi d_p^{\,2}}{4} \tag{S7}$$

This value is constant for all different regimes as the particle size is constant. However, the required area for a particle to deposit is different for different regimes. In the ballistic regime, the advective velocity is dominant and particle deposits on a straight orthogonal trajectory to the surface due to the high advective velocity. In this case, the collision area for a particle to deposition on the surface before colliding with any other particle can be calculated as follows:

$$A_{stat} = \pi d_p^{\,2} \tag{S8}$$

Despite different mechanism for particle deposition, this is the minimum area a particle requires to deposit on the surface without touching any other ones. The lowest porosity of the ballistic films and the highest SD (Fig. 4a, main text) are attributed to this minimum collision area required for particle (Fig. S6a) when the particle dynamic is dominated by high advective velocity. In the randomly oriented ballistic regime, the particle is sufficiently small (d_p < 10 nm) and touches the surface on a single Brownian displacement (Fig. S6b). The collision area calculated for these particles is the sum of the minimal area required for particle deposition (A_{stat}) and the additional horizontal area swept by a particle due to the Brownian displacement, X, within the potential collision length, d_p, (A_{dyn}). Thus, the collision area is calculated from the following equation (Fig. 5b, insets):

$$A_{stat} + A_{dyn} = \pi d_p^{\ 2} + (2d_p X - A_{over}) \tag{S9}$$

where A_{over} is the area overlapped between the minimal area required for deposition and that due to single-step Brownian displacement (Fig. 5b, insets) which can be calculated as below:

$$A_{over} = 2\int_0^X (d_p^{\ 2} - y^2)dy = X\sqrt{(d_p^{\ 2} - X^2)} + d_p^{\ 2}\sin^{-1}(\frac{X}{d_p}) \tag{S10}$$

$$A_{over} = d_p^{\ 2}\left[\overline{X}\sqrt{(1-\overline{X}^2)} + \sin^{-1}(\overline{X})\right] \tag{S11}$$

The collision area of a particle in randomly oriented ballistic regime is calculated using equations (S9) and (S11):

$$A_{stat} + A_{dyn} = d_p^{\ 2}\left[\pi + 2\overline{X} - \overline{X}\sqrt{1-\overline{X}^2} + \sin^{-1}(\overline{X})\right] \tag{S12}$$

This results in a scaled particle surface density (SD) equal to:

$$SD = \frac{A_{dp}}{A_{stat} + K_{RPF}A_{dyn}} \tag{S13}$$

where the K_{RPF} is the Randomly Path Factor and for a single-step Brownian displacement is equal to 1.

$$SD = \frac{\pi}{4\left[\pi + 2\overline{X} - \left[\overline{X}\sqrt{1-\overline{X}^2} + \sin^{-1}(\overline{X})\right]\right]} \tag{S14}$$

For the diffusion regime, the amount of Brownian steps increases due to the particle mean free path (λ_{dp}) becoming smaller in the collision length (Fig. S6d, e and Fig. 4b, main text). The obtained K_{RPF} factors resulting in an s-shaped profile between particle size (Supplementary Fig. 6d) and particle mean free path (Fig. 5e) as a function of K_{RPF} factor.

VI. Computation of the Brownian Displacement through the Collision Length

The Brownian's motion induced horizontal displacement within the vertical collision length (d_p) was computed from the average transition time as a function of particle size and Péclet-number:

$$v.t + X = d_p \tag{S15}$$

where v is the particle velocity, t is the time, X is the Brownian displacement and d_p is the particle diameter. Following the Stokes-Einstein equation, the distance travelled by a particle suspended in a fluid is related to the diffusion coefficient of the particle in that fluid, D, and the travelled time, t:

$$X = \sqrt{2Dt} \tag{S16}$$

This leads to:

$$d_p{}^2 - (2d_p v + 2D)t + v^2 t^2 = 0 \tag{S17}$$

Solution of quadratic equation results in a transition time, (t), :

$$t = \frac{d_p}{v} + \frac{D}{v} - \frac{\sqrt{D^2 + 2d_p.v.D}}{v^2} \tag{S18}$$

By replacing this time in equation (S17), we obtained an average Brownian displacement, (X),:

$$X^2 = \frac{2d_p D}{v} + \frac{D^2}{v^2} - \frac{2D\sqrt{D^2 + 2d_p vD}}{v^2} \tag{S19}$$

Considering the Péclet-number definition:

$$Pe = \frac{(d_p/2)v}{D} \tag{S20}$$

This leads to a Brownian displacement, *X*, equal to (Fig. S7):

$$X = d_p \sqrt{\frac{1}{Pe} + \frac{1}{2Pe^2} - \frac{1}{2Pe^2}\sqrt{1+4Pe}} \tag{S21}$$

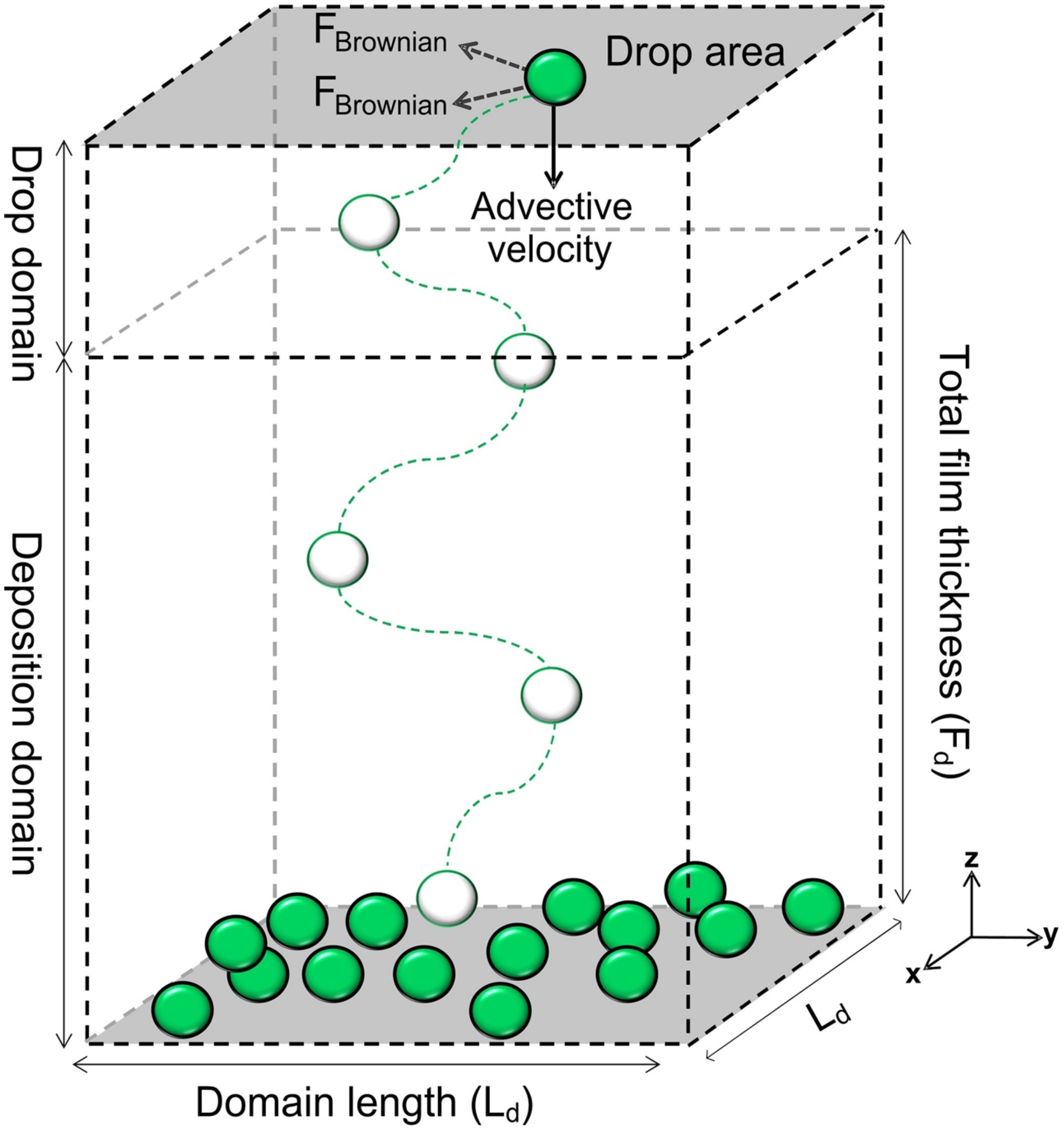

Figure S1. Schematic of the simulated domain and deposition conditions for nanoparticles on a flat substrate reaching a constant film thickness. Particles are inserted at the drop point and flow downstream.

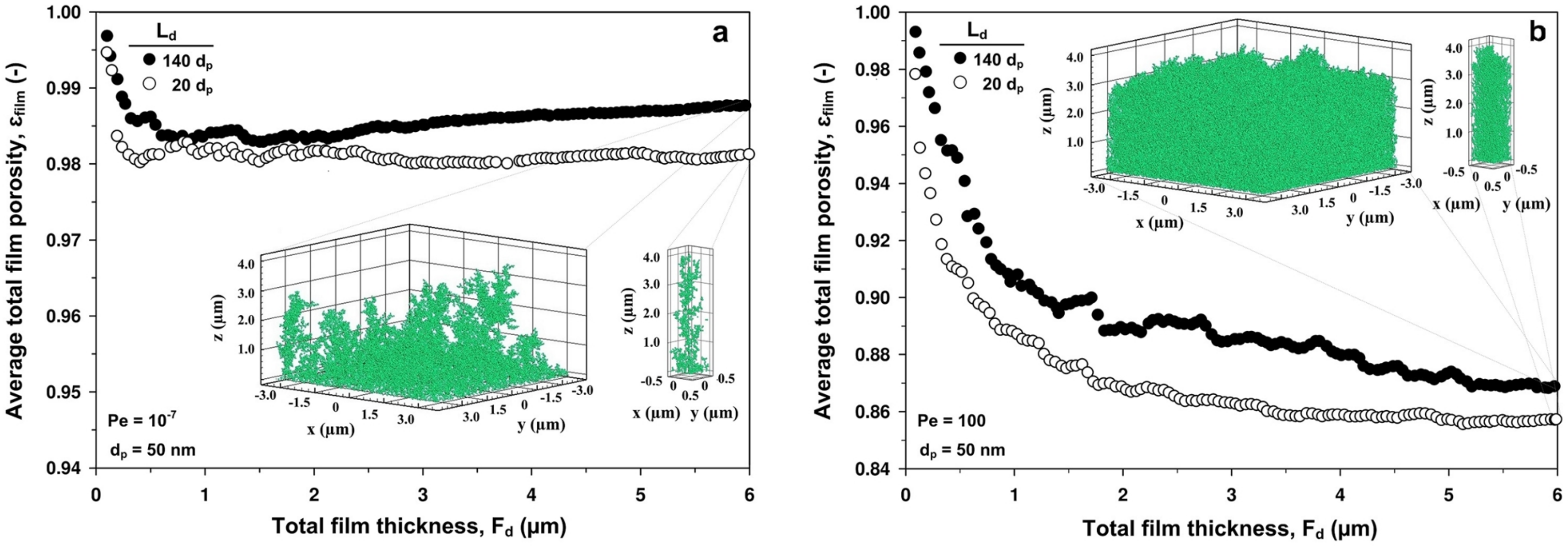

Figure S2. Average film porosity (ε_{film}) as a function of total film thickness (F_d) with particle diameter of 50 nm and two domain lengths ($30d_p$ and $140d_p$) in the **a**, diffusion and **b**, ballistic regime.

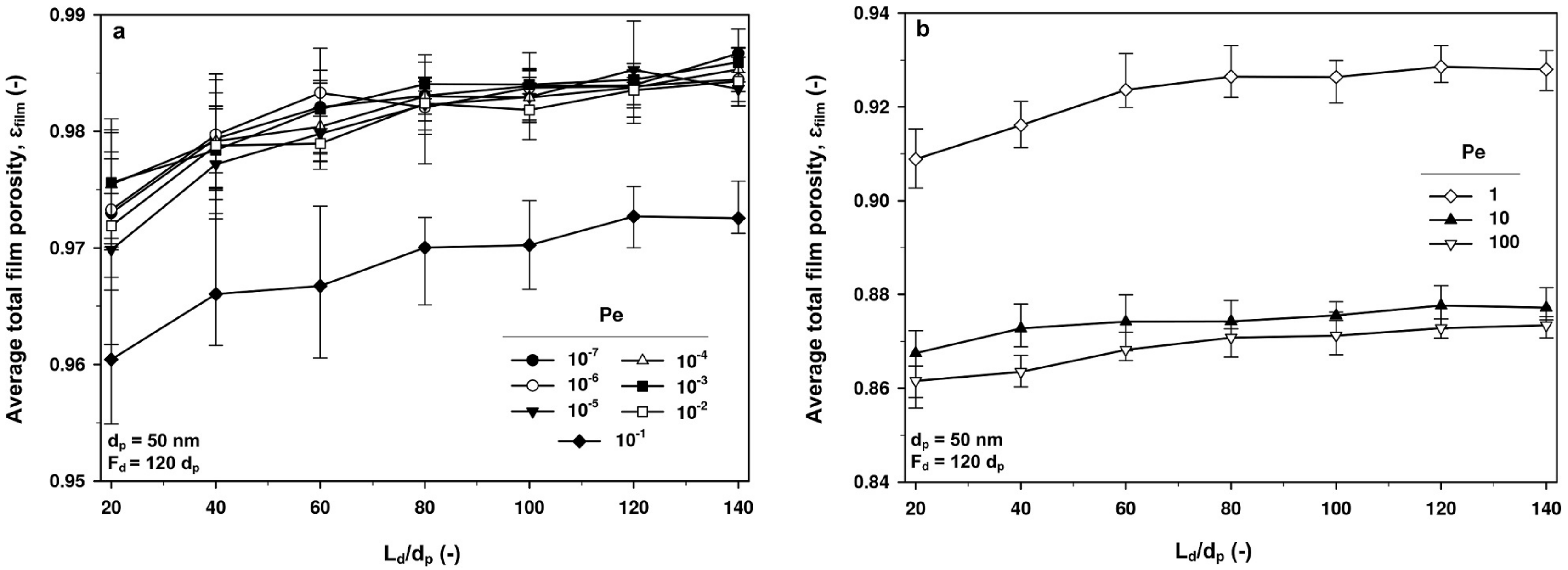

Figure S3. Average film porosity (ε_{film}) for spherical nanoparticles with a diameter of 50 nm as a function of domain length ($20d_p$ to $140d_p$) from **a**, diffusion to the **b**, ballistic regime.

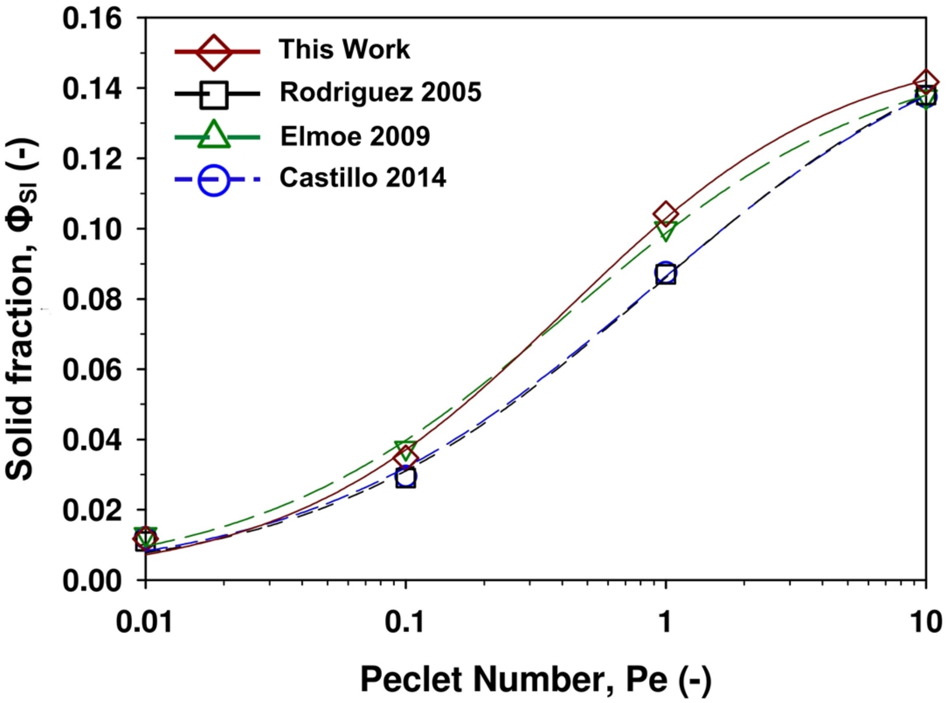

Figure S4. Plateau solid fraction as a function of the Pe number for deposition of single spherical particles of 50 nm in diameter by this work (diamond) and comparison with previous researches obtained for flat deposition surfaces[23,28] (rectangles and circle) and capillary[27] (triangles).

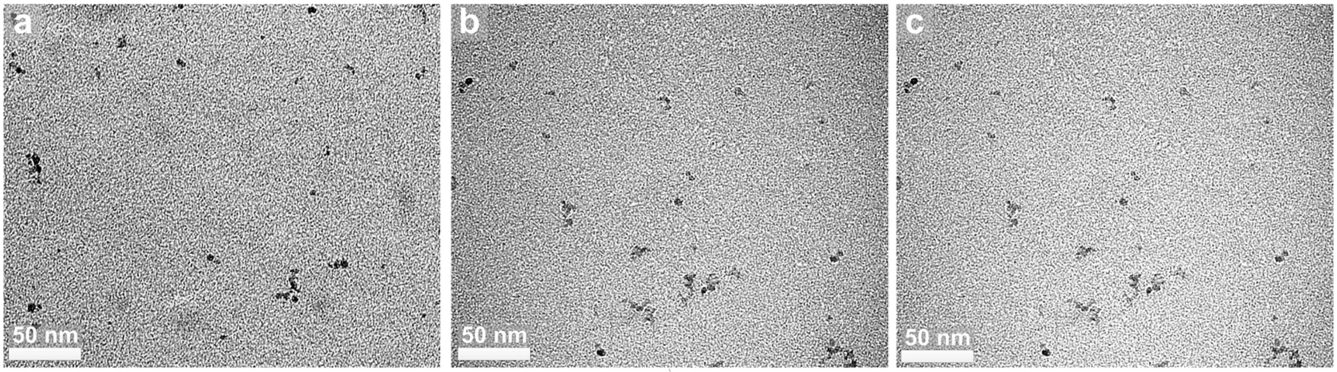

Figure S5. TEM images of quasi-non-agglomerated TiO_2 particles collected from the flame spray pyrolysis-generated aerosols on TEM grids.

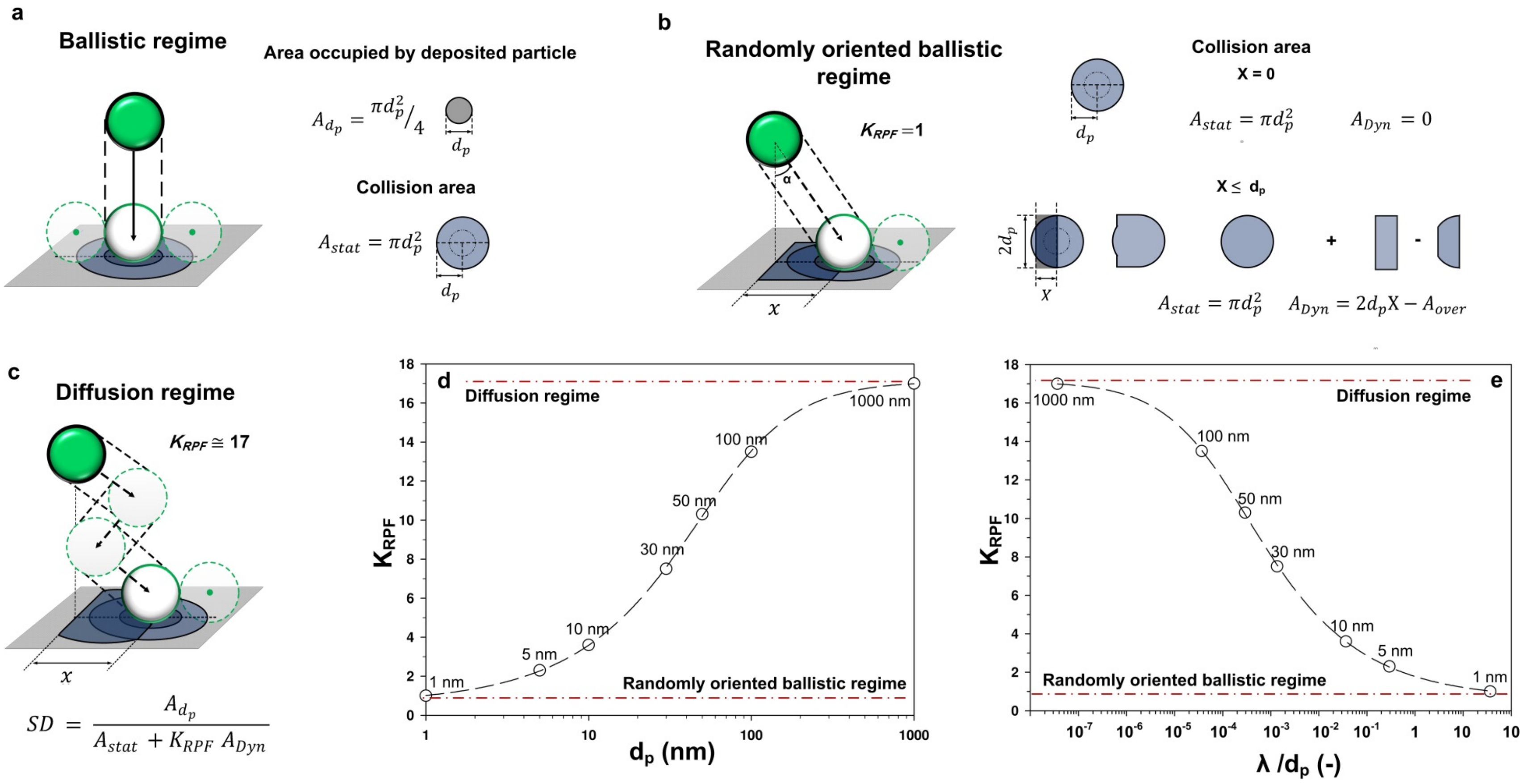

Figure S6. Different deposition mechanism and scaled particle surface density in (a) ballistic, (b) randomly oriented ballistic and c, diffusion regime as a function of the (d) particle diameter and (e) mean free path. The increase in travelled path for diffusive particle ($\lambda_p/d_p<1$) is accounted through the K_{RPF} factor as discussed in details in the analytical model section.

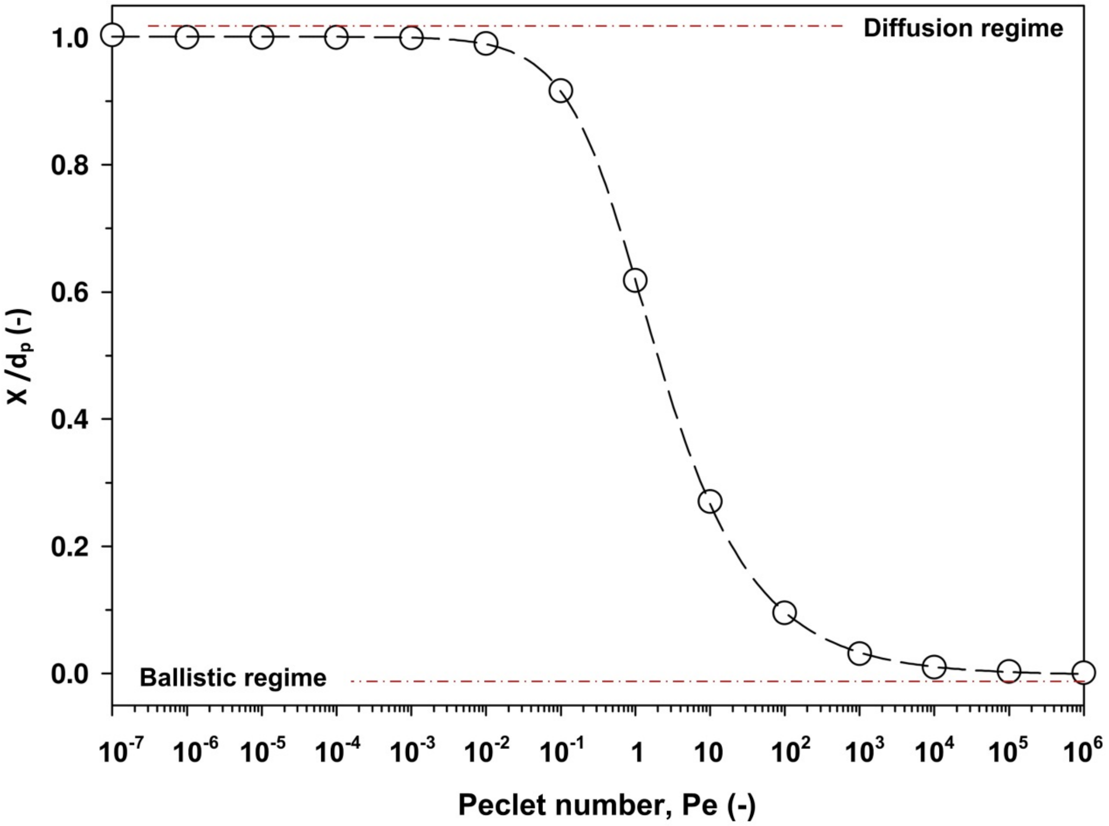

Figure S7. Brownian displacement to the collision length (d_p) ratio as a function of Péclet-number.